Small mass- and trap-imbalanced two-component Fermi systems

D. Blume[1]

[1]*Department of Physics and Astronomy, Washington State University, Pullman, Washington 99164-2814*

(Dated: March 28, 2008)

Motivated by the prospect of optical lattice experiments with two-component Fermi gases consisting of different atomic species such as Li and K, we calculate the energies for N fermions under harmonic confinement as a function of the mass- and trap-imbalance, i.e., as a function of the ratio between the masses and frequencies of species one and two, using microscopic approaches. Our energies for $N = 2$ through 6 can be used to determine the energetically most favorable configuration for a given number of atoms per species of a deep lattice in which each lattice site is approximately harmonic and in which tunneling between neighboring sites can be neglected. Furthermore, our energies determine one of the input parameters, namely the onsite interaction strength, of the corresponding lattice Hamiltonian. We also determine and interpret the excitation gap for unequal-mass systems with up to $N = 13$ atoms for equal oscillator lengths.

PACS numbers:

I. INTRODUCTION

Cold-atom experiments have reached an impressive level of sophistication over the past decade. About ten different atomic species have been Bose condensed and, although experimentally more challenging, an increasing number of fermionic species have been cooled to quantum degeneracy, including ^{3}He [1], ^{6}Li [2], ^{40}K [3] and two Yb isotopes (^{171}Yb and ^{173}Yb) [4, 5]. To date, experiments on fermionic atoms have focused on studying Bose-Fermi mixtures [6, 7, 8, 9], one-component Fermi systems with p-wave interactions [10] and equal-mass two-component Fermi systems with interspecies s-wave interactions [11, 12, 13].

Presently, the simultaneous trapping and cooling of two different fermionic species is being actively pursued by a number of laboratories [14, 15, 16], adding a new degree of freedom, i.e., the mass ratio between the two atomic species. Unequal-mass two-component Fermi systems are expected to behave quite differently than the equal-mass counterpart [17, 18, 19, 20, 21, 22, 23, 24, 25, 26]. From the few-body perspective, the existence of weakly-bound trimers for sufficiently large mass ratios consisting of two heavy fermions and one light fermion is intriguing [17, 18, 19, 20]. Whether the existence of these bound trimer states allows, e.g., for the formation of a gas consisting of trimers with sufficiently long lifetime has been discussed [27]. On the other hand, adopting a many-body perspective [21, 22, 23, 26], the ground state phase diagram of mass- and population-imbalanced two-component Fermi systems has been predicted to show quantum and topological phase transitions which are not present in the phase diagram of population-balanced equal-mass two-component Fermi systems.

The increasing interest of not only the atomic physics community but also the nuclear physics, molecular physics, condensed matter physics and quantum information science communities in cold atom systems can be attributed to two major achievements. First, the atom-atom scattering length can be adjusted experimentally to essentially any value, including vanishingly small and infinitely large positive or negative values, by applying an external field in the vicinity of a so-called Fano-Feshbach resonance [28, 29, 30, 31]. Second, cold atomic gases can be loaded into an optical lattice [32, 33, 34, 35], allowing, e.g., for the study of the Mott-insulator transition [32], a topic historically primarily considered by condensed matter physicists. Furthermore, cold atom systems loaded into optical lattices may ultimately be used as a quantum simulator [36, 37, 38].

To date, most microscopic studies of equal-mass systems have assumed equal trapping potentials of the two species [39, 40, 41, 42, 43, 44, 45, 46]. However, the lattice potential felt by the two different hyperfine states may be different even for equal-mass systems, leading to trap-imbalanced systems [47]. For unequal-mass systems such as a ^{6}Li-^{40}K mixture (for which the mass ratio κ is approximately 6.7), the trapping potentials felt by the two species are, in general, different, owing to the mass difference and the species-dependent properties of the hyperfine states. The trapping potentials felt by the two species may be tuned to some degree experimentally [24, 47]. Motivated by these considerations, the present paper explores the rich behavior of trap- and mass-imbalanced systems. These systems share some similarities with population-imbalanced systems [48, 49], which have received considerable attention recently.

Assuming a deep lattice with neglegibly small tunneling between neighboring lattice sites, this paper determines the ground state properties of small s-wave interacting two-component Fermi systems trapped by spherically symmetric harmonic species-specific potentials with trapping frequencies ω_1 and ω_2, respectively. Throughout, we adopt a microscopic many-body framework. Our main results are: (i) For small but negative s-wave scattering lengths, we determine a compact expression for the ground state energy of small systems with unequal masses and trapping frequencies perturbatively. (ii) In the strongly-interacting unitary regime, our numerical energies determine the phase diagram of optical lattice

systems in the no-tunneling regime for a large range of mass ratios and trapping frequencies and the on-site interaction strengths that parametrize the corresponding lattice Hamiltonian; furthermore, they provide insights into the behavior of the excitation gap. (iii) We show explicitly that the behavior of trap-imbalanced systems with small and positive s-wave scattering lengths is—just as that of trap-balanced systems—to leading order governed by the dimer-dimer scattering length.

Section II introduces the Hamiltonian and the numerical techniques employed to solve the corresponding time-independent Schrödinger equation. Section III contains our results for small negative, infinitely large and small positive s-wave scattering lengths. Finally, Sec. IV concludes.

II. THEORETICAL BACKGROUND

A. Hamiltonian

The adopted model Hamiltonian H for a two-component Fermi system with N_1 mass m_1 and N_2 mass m_2 atoms under spherically harmonic confinement reads

$$H = \sum_{i=1}^{N_1} \left(\frac{-\hbar^2}{2m_1} \nabla_i^2 + \frac{1}{2} m_1 \omega_1^2 \vec{r}_i^{\,2} \right) + \sum_{i'=1}^{N_2} \left(\frac{-\hbar^2}{2m_2} \nabla_{i'}^2 + \frac{1}{2} m_2 \omega_2^2 \vec{r}_{i'}^{\,2} \right) + \sum_{i=1}^{N_1} \sum_{i'=1}^{N_2} V(\vec{r}_{ii'}), \quad (1)$$

where $\vec{r}_i$ and $\vec{r}_{i'}$ denote the position vectors of the ith atom of species 1 and the i'th atom of species 2, respectively, and ω_1 and ω_2 the angular trapping frequencies felt by the atoms of species 1 and 2, respectively. The interaction potential V depends on the interparticle distance vector $\vec{r}_{ii'}$, $\vec{r}_{ii'} = \vec{r}_i - \vec{r}_{i'}$, and is characterized by the s-wave scattering length a_s. Throughout, like atoms are assumed to be non-interacting, which is well justified for most experimentally relevant systems.

Our perturbative, small $|a_s|$ analysis (see Sec. III A) considers a zero-range δ-function potential $V_\delta(\vec{r})$ [50],

$$V_\delta(\vec{r}) = \frac{2\pi\hbar^2 a_s}{\mu} \delta(\vec{r}), \quad (2)$$

where μ denotes the reduced mass, $\mu = m_1 m_2/(m_1 + m_2)$. In our numerical calculations (see Secs. III B and III C) we employ, as in our previous calculations [44, 45, 46], a shape-dependent spherically-symmetric square well potential $V_{sw}(r)$ with range R_0 and depth V_0 ($V_0 > 0$),

$$V_{sw}(r) = \begin{cases} -V_0 & \text{for } r < R_0 \\ 0 & \text{for } r > R_0 \end{cases}, \quad (3)$$

where $r = |\vec{r}|$. For a fixed R_0, V_0 is adjusted so that the interspecies s-wave scattering length a_s takes on the desired value. Section III B considers the so-called unitary regime, where V_0 is adjusted so that the two-body potential supports a zero-energy s-wave bound state, implying a diverging s-wave scattering length a_s, i.e., $1/a_s = 0$, but no deeply-lying bound states. Section III C, in contrast, considers the regime where V_0 is adjusted so that the free-space dimer supports one deep-lying s-wave bound state (whose binding energy depends on the details of the two-body potential), implying a small positive s-wave scattering length. The range R_0 of V_{sw} is taken to be small compared to the oscillator lengths $a_{ho,i}$,

$$a_{ho,i} = \sqrt{\hbar/(m_i \omega_i)}, \quad (4)$$

where $i = 1$ or 2. Most calculations reported below use $R_0 = 0.01 a_{ho,1}$. To estimate how well the resulting properties agree with those for zero-range interactions, we analyze the dependence of the observables on the range R_0 in detail for a few selected cases.

Section III presents our results for three different scattering length regimes, i.e., for weakly-attractive Fermi gases ($|a_s|$ small and $a_s < 0$), for strongly-interacting Fermi gases ($1/|a_s| = 0$) and for weakly-repulsive Fermi gases (a_s small and $a_s > 0$). In all three regimes, we determine the energies of small trapped systems with either $N_1 = N_2$ or $|N_1 - N_2| = 1$. In addition to changing the number of particles and the scattering length a_s, we vary the mass ratio κ,

$$\kappa = m_2/m_1, \quad (5)$$

and the ratio ω_2/ω_1 between the two trapping frequencies. Mass ratios ranging from $\kappa = 1$ to 8 are considered (for unequal-mass systems species 2 has the heavier mass). For $\kappa \gtrsim 8.6$, three-body bound states have been predicted to exist for systems that consist of two heavy fermions and one light fermion and that interact through zero-range potentials [19, 20]. While studying the implications of these three-body states for many-body systems is interesting (see, e.g., Ref. [27]), this topic is beyond the scope of the present paper.

B. Numerical techniques

To solve the time-independent Schrödinger equation for the Hamiltonian given in Eq. (1), we employ two different numerical techniques. For $N_1 = N_2 = 1$, we first build and then diagonalize the Hamiltonian matrix while we resort to the fixed-node diffusion quantum Monte Carlo (FN-DMC) technique [51, 52] for larger systems.

We first discuss the diagonalization approach employed to solve the Schrödinger equation for the Hamiltonian given in Eq. (1) with $N_1 = N_2 = 1$ and $V = V_{sw}$; it follows Ref. [53], with the main difference that we use a finite-range square-well potential while Ref. [53] uses the Fermi-Huang pseudo-potential [54]. We rewrite our two-body Hamiltonian H_{tb} in terms of a center-of-mass Hamiltonian H_{cm}, a relative Hamiltonian H_{rel} and a cou-

pling term $V_{coup}(\vec{R},\vec{r})$ [53],

$$H_{tb} = H_{cm} + H_{rel} + V_{coup}(\vec{R},\vec{r}), \tag{6}$$

where

$$H_{cm} = \frac{-\hbar^2}{2M}\nabla^2_{\vec{R}} + \frac{1}{2}M\omega^2_{cm}R^2, \tag{7}$$

$$H_{rel} = \frac{-\hbar^2}{2\mu}\nabla^2_{\vec{r}} + \frac{1}{2}\mu\omega^2_{rel}r^2, \tag{8}$$

and

$$V_{coup}(\vec{R},\vec{r}) = \mu\omega^2_{coup}\vec{R}\cdot\vec{r}. \tag{9}$$

Here, $\vec{R}$ and $\vec{r}$ ($\vec{r} = \vec{r}_1 - \vec{r}_2$) denote the center-of-mass and relative vectors, respectively, and M denotes the total mass of the two-body system, $M = m_1 + m_2$. The frequencies ω_{cm}, ω_{rel} and ω_{coup} are defined as

$$\omega_{cm} = \sqrt{(m_1\omega_1^2 + m_2\omega_2^2)/M}, \tag{10}$$

$$\omega_{rel} = \sqrt{(m_2\omega_1^2 + m_1\omega_2^2)/M} \tag{11}$$

and

$$\omega_{coup} = \sqrt{|\omega_1^2 - \omega_2^2|}. \tag{12}$$

For equal trapping frequencies, V_{coup} vanishes and both ω_{cm} and ω_{rel} reduce to ω_1 (which equals ω_2). In this case, the center-of-mass and relative motions decouple, and the total wave function $\Psi(\vec{R},\vec{r})$ can be written as a product of a $\vec{R}$-dependent function Φ_{NLM_L} and a $\vec{r}$-dependent function ϕ_{nlm_l}. The Φ_{NLM_L} and ϕ_{nlm_l} are solutions to the Schrödinger equations for H_{cm} and H_{rel}, respectively, and the subscripts NLM_L and nlm_l denote the principal, angular momentum and projection quantum numbers of the center-of-mass and relative systems, respectively. The Φ_{NLM_L} are the harmonic oscillator wave functions of a mass M particle with eigenenergies E_{NL},

$$E_{NL} = \left(2N + L + \frac{3}{2}\right)\hbar\omega_{cm}, \tag{13}$$

where $N = 0, 1, \cdots$, $L = 0, 1, 2, \cdots$ and $M_L = -L, -L+1, \cdots, L$. For the spherically-symmetric square well potential V_{sw}, the angular part of the relative wave function ϕ_{nlm_l} is given by the spherical harmonic Y_{lm_l} while the radial part R_{nl} can be written in terms of the confluent hypergeometric function M for $r < R_0$ and the Kummer function U for $r > R_0$ (see, e.g., Ref. [55]). Equating the log-derivative of the inner and outer radial wave functions at $r = R_0$ results in a compact expression for the eigenequation, from which we obtain the eigenenergies E_{nl} of H_{rel} using standard root-finding techniques. The radial wave functions R_{nl} are then readily obtained by enforcing continuity at $r = R_0$. We normalize the $R_{nl}(r)$ numerically.

To determine the eigenenergies of the two-particle Hamiltonian H_{tb} with non-zero $V_{coup}(\vec{R},\vec{r})$, we expand the full wave function $\Psi(\vec{R},\vec{r})$ in terms of the complete set $\{\Phi_{NLM_L}(\vec{R})\phi_{nlm_l}(\vec{r})\}$. Recognizing that H_{tb} commutes with the z-component of the total angular momentum operator (i.e., that $M_L + m_l$ is conserved), we restrict the allowed M_L and m_l combinations to $M_L + m_l = 0$. Since the Φ_{NLM_L} and ϕ_{nlm_l} are solutions of H_{cm} and H_{rel}, respectively, H_{cm} and H_{rel} are diagonal in this representation. To evaluate the matrix elements involving V_{coup}, we rewrite the dot product $\vec{R}\cdot\vec{r}$ in terms of R, r, and the spherical harmonics $Y_{L=1,M_L}$ and $Y_{l=1,m_l}$ associated with the center-of-mass and relative degrees of freedom, respectively. The angular integrals then readily reduce to Clebsch Gordon coefficients (multiplied by trivial constants), and the radial integrals are performed numerically. The number of basis functions needed to converge the ground state energy to a given relative accuracy strongly depends on the interaction strength considered. At unitarity, e.g., we need a larger basis set than in the regime where a_s is small and positive (see Secs. III B and III C).

The computational effort of diagonalization schemes such as that outlined above increases dramatically with increasing number of particles, and eventually becomes computationally unfeasible. For larger number of particles, we thus resort to an alternative numerical approach, the FN-DMC method [51, 52], which exhibits a more favorable scaling with increasing number of particles. Our implementation of the FN-DMC method has been discussed in detail in two recent papers [45, 46]; here, we only review the key points.

The FN-DMC technique, as used throughout this paper, determines an approximate energy of the many-body system whose corresponding eigenfunction has the same symmetry as a so-called guiding function ψ_T, i.e., the FN-DMC technique determines the energy of a state that has the same nodal surface as ψ_T but that may differ from ψ_T in other regions of the configuration space. If the nodal surface of ψ_T coincides with that of the true eigenfunction, then the FN-DMC method results—within the statistical uncertainty that stems from the stochastic nature of the approach—in the exact eigenenergy. If the nodal surface of ψ_T differs from that of the true eigenfunction, then the FN-DMC method results in an upper bound to the true eigenenergy whose eigenstate has the same symmetry as ψ_T. For example, ψ_T can be constructed so as to obtain an upper bound for the lowest eigen energy with total angular momentum $L_{tot} = 0$ or 1 [46]. In this paper, we restrict our FN-DMC calculations to the energetically lowest-lying gas-like state of the system.

We consider three different parametrizations of the guiding function ψ_T: (i) A guiding function ψ_{T1} whose nodal surface is constructed by anti-symmetrizing a pair

function. If N is odd, a single-particle orbital is added (with the proper anti-symmetrization). The detailed functional form of ψ_{T1} is given by Eqs. (35)-(39) of Ref. [46]. (ii) A guiding function ψ_{T2} whose nodal surface coincides with that of the non-interacting ideal-gas nodal surface for the same number of fermions of species 1 and species 2. The parametrization follows that given by Eq. (40) of Ref. [46]. (iii) A guiding function ψ_{T3} whose functional form allows, at least in principle, to interpolate between the nodal surfaces of ψ_{T1} and ψ_{T2}. The functional form is given by Eqs. (3)-(4) of Ref. [43].

III. RESULTS

A. Small negative s-wave scattering length

This section considers the properties of small two-component Fermi systems with unequal masses and unequal trapping frequencies in the weakly-attractive regime, where $|a_s|$ is small ($a_s < 0$). In this regime, a compact expression for the ground state energy of the Hamiltonian given in Eq. (1) can be determined within first order degenerate perturbation theory for the Fermi pseudo-potential V_δ, Eq. (2). Denoting the energy of the non-interacting system with N_1 atoms of mass m_1 and N_2 atoms of mass m_2 by $E^{NI}_{N_1,N_2}$ (see Table I for selected values), the perturbative expression for the energy E_{N_1,N_2} reads

$$E_{N_1,N_2} \approx E^{NI}_{N_1,N_2} + \hbar\bar{\omega}\frac{a_s}{\bar{a}_{ho}} C_{N_1,N_2}, \qquad (14)$$

where

$$\bar{\omega} = \frac{M\omega_1\omega_2}{m_1\omega_1 + m_2\omega_2} \qquad (15)$$

and

$$\bar{a}_{ho} = \sqrt{\frac{\hbar}{2\mu\bar{\omega}}} = \sqrt{\frac{a^2_{ho,1} + a^2_{ho,2}}{2}}. \qquad (16)$$

The quantities $\bar{\omega}$ and $\bar{a}_{ho}$ have been defined so that the coefficient $C_{1,1}$ is constant (i.e., independent of η, see below). We refer to $\bar{\omega}$ and $\bar{a}_{ho}$ as the "natural angular trapping frequency" and the "natural oscillator length" of the two-body system in the BCS regime.

The coefficients C_{N_1,N_2} are listed in Table I for selected N_1 and N_2 combinations with $|N_1 - N_2| = 0$ or 1 ($N \leq 8$). They reduce to those reported in Ref. [46] for equal masses and equal frequencies. The coefficients C_{N_1,N_2} in Table I are written in terms of $a_{ho,1}$ and $a_{ho,2}$; alternatively, they can be written in terms of η,

$$\eta = 1 - \left(\frac{a_{ho,2}}{a_{ho,1}}\right)^2. \qquad (17)$$

The quantity η measures the density imbalance of the non-interacting two-component Fermi gas. For $\eta = 0$, the oscillator lengths $a_{ho,i}$ ($i = 1$ and 2) coincide; for closed shell systems with $N_1 = N_2$, this implies fully overlapping densities of the two non-interacting components. For $\eta < 0$, we have $a_{ho,2} > a_{ho,1}$, while for $\eta > 0$, we have $a_{ho,2} < a_{ho,1}$. For $\kappa = 4$, e.g., $\eta < 0$ corresponds to $\omega_2 < \omega_1/4$ and $\eta > 0$ corresponds to $\omega_2 > \omega_1/4$.

Figure 1 shows the dimensionless coefficients C_{N_1,N_2} for $N \leq 8$ as a function of η. Plotted this way, the coefficients C_{N_1,N_2} for fixed N_1, N_2 and η but different κ collapse to a single curve. For $N = 2$, C_{N_1,N_2} is constant (see above). For $N = 4$, C_{N_1,N_2} is maximal for $\eta = 0$ and decreases as $|\eta|$ increases. This implies that the attractive interspecies scattering length a_s can most effectively introduce correlations that lead to a lowering of the energy, compared to $E^{NI}_{N_1,N_2}$, when the densities of the two components overlap fully. For $N = 3$, the coefficient $C_{2,1}$

TABLE I: Energies $E^{NI}_{N_1,N_2}$ of the non-interacting system and dimensionless coefficients C_{N_1,N_2} that determine the ground state energy of weakly-attractive trap- and mass-imbalanced two-component Fermi gases for selected N_1 and N_2 values. The subscript pair (j,k) can take the values $(1,2)$ or $(2,1)$.

N_j	N_k	$E^{NI}_{N_1,N_2}/\hbar$	$C_{N_j,N_k} \times (2\sqrt{2\pi})$
1	1	$\frac{3}{2}(\omega_j + \omega_k)$	4
2	1	$4\omega_j + \frac{3}{2}\omega_k$	$(2a^2_{ho,j} + 4a^2_{ho,k})/\bar{a}^2_{ho}$
2	2	$4(\omega_j + \omega_k)$	$(2a^4_{ho,j} + 9a^2_{ho,j}a^2_{ho,k} + 2a^4_{ho,k})/\bar{a}^4_{ho}$
3	2	$\frac{13}{2}\omega_j + 4\omega_k$	$(2a^4_{ho,j} + 10a^2_{ho,j}a^2_{ho,k} + 3a^4_{ho,k})/\bar{a}^4_{ho}$
3	3	$\frac{13}{2}(\omega_j + \omega_k)$	$(3a^4_{ho,j} + 16a^2_{ho,j}a^2_{ho,k} + 3a^4_{ho,k})/\bar{a}^4_{ho}$
4	3	$9\omega_j + \frac{13}{2}\omega_k$	$(3a^4_{ho,j} + 17a^2_{ho,j}a^2_{ho,k} + 4a^4_{ho,k})/\bar{a}^4_{ho}$
4	4	$9(\omega_j + \omega_k)$	$(4a^4_{ho,j} + 23a^2_{ho,j}a^2_{ho,k} + 4a^4_{ho,k})/\bar{a}^4_{ho}$

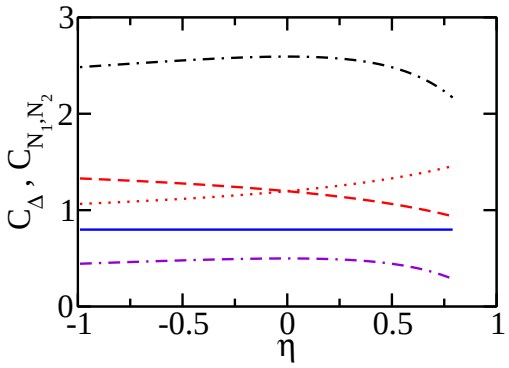

FIG. 1: (Color online) Dimensionless coefficients $C_{1,1}$ (solid line), $C_{2,1}$ (dashed line), $C_{1,2}$ (dotted line) and $C_{2,2}$ (dash-dotted line) as a function of η for weakly-attractive two-component Fermi gases. The dash-dash-dotted line shows the dimensionless quantity C_Δ, Eq. (20), which determines the excitation gap $\Delta(N)$ for $N = 3$, 5 and 7.

decreases with increasing η while the coefficient $C_{1,2}$ increases with increasing η. This "asymmetry" can be understood by realizing that the maximal density overlap of the two components for odd-N systems occurs for finite η and not for $\eta = 0$. For $N_1 = 2$ and $N_2 = 1$, e.g., the maximal density overlap of the non-interacting system occurs for $\eta < 0$; consequently, the $C_{2,1}$ coefficient decreases with increasing η. For $N_1 = 1$ and $N_2 = 2$, in contrast, the maximal density overlap of the non-interacting system occurs for $\eta > 0$. This explains the reversed behavior of $C_{2,1}$ and $C_{1,2}$ as a function of η.

The energies for systems with even and odd total number of atoms determine the excitation gap $\Delta(N)$ (see, e.g., Ref. [56]),

$$\Delta(N) = \frac{E_{(N-1)/2,(N+1)/2} + E_{(N+1)/2,(N-1)/2}}{2} - \frac{E_{(N-1)/2,(N-1)/2} + E_{(N+1)/2,(N+1)/2}}{2}, \quad (18)$$

where we have taken N to be odd. Using the perturbative energy expression, Eq. (14), we find

$$\Delta(N) \approx -\hbar\bar{\omega}\frac{a_s}{\bar{a}_{ho}}C_\Delta, \quad (19)$$

where

$$C_\Delta = \frac{1}{4\sqrt{2\pi}}\,\frac{5a_{ho,1}^2 a_{ho,2}^2}{\bar{a}_{ho}^4} \quad (20)$$

for $N = 3$, 5 and 7. The excitation gap determined perturbatively is independent of N for $N \leq 7$ for all m_i and ω_i combinations. A dash-dash-dotted line in Fig. 1 shows C_Δ as a function of η. The coefficient C_Δ, and consequently also $\Delta(N)$, is largest for $\eta = 0$ and decreases with increasing $|\eta|$. This can be readily understood by realizing that the energies for odd-N systems [first term on the right hand side of Eq. (18)] average to a constant, and that the average of the energies for even-N system [second term on the right hand side of Eq. (18)] is minimal for $\eta = 0$.

The equal-frequency systems with mass ratio κ correspond to $\eta = (\kappa - 1)/\kappa$. Figure 1 shows that the coefficient C_Δ decreases with increasing mass ratio κ for systems with $\omega_1 = \omega_2$, in agreement with the findings of Ref. [46].

B. Infinitely large s-wave scattering length

This section considers infinitely strongly interacting two-component Fermi systems with diverging s-wave scattering length a_s and varying mass and frequency ratios. Throughout this section, we express energies in units of the average oscillator energy $\hbar\omega$,

$$\hbar\omega = \frac{\hbar\omega_1 + \hbar\omega_2}{2}; \quad (21)$$

this unit is convenient since the energies of the non-interacting systems with $N_1 = N_2$ are directly proportional to $\hbar\omega$ (see, e.g., Table I for small N). For $N = 3 - 14$ atoms, we determine the eigenenergies of the stationary Schrödinger equation by the FN-DMC method. For $N = 2$, we compare the diffusion Monte Carlo (DMC) energies (in this case, the ground state of the system is nodeless and no nodal approximation needs to be made) with the energies obtained from the diagonalization scheme.

Table II reports selected two-body energies ($N_1 = N_2 = 1$) for $\kappa = 1$, 4 and 8 at unitarity. The energies in the third and fourth column are calculated for the square well potential with $R_0 = 0.01a_{ho,1}$ using the DMC and the diagonalization approaches, respectively. We analyzed the convergence of the energies obtained by the diagonalization approach by considering basis sets with up to about 1000 basis functions. Within the statistical uncertainties of the DMC energies, the values reported in columns three and four agree. To estimate the energy's dependence on the range R_0 of the square well potential, we diagonalize the Hamiltonian matrix for different R_0. We find that the energies for fixed ratio and frequency ratios vary linearly with R_0, allowing for a simple linear extrapolation to the $R_0 \to 0$ limit (see Ref. [46] for a similar analysis of equal-frequency systems). The energies for $R_0 = 0.01a_{ho,1}$ are slightly larger than the extrapolated zero-range energies (seventh column of Table II) for all mass and frequency ratios considered, and deviate by less than 0.5% from the extrapolated zero-range energies. Our extrapolated two-body energies at unitarity for equal frequencies equal $2\hbar\omega$ for all κ, in agreement with analytical results for the zero-range potential [57]. For larger systems (see below) we do not explicitly extrapolate to the zero-range limit. Based on our two-body results, we estimate that the finite range effects of the FN-DMC energies for the larger systems at unitarity are at most about a few times larger than the statistical uncertainties.

Figure 2(a) shows the two-body energies $E_{1,1}$ calculated by the DMC method for the square well potential with $R_0 = 0.01a_{ho,1}$ and $1/|a_s| = 0$ for $\kappa = 1, 2, 4, 6$ and 8 as a function of η. For equal masses, Fig. 2(a) shows the energies for frequency ratios ω_2/ω_1 ranging from 1/2 to 1. For unequal masses, the ratio ω_2/ω_1 of trapping frequencies shown ranges from values a bit smaller than κ^{-1} to 1. In units of $\hbar\omega$, the two-body energies for a fixed η decrease with increasing mass ratio κ. Furthermore, the minimum of the $E_{1,1}$ curves moves to larger η as κ increases.

To shed further light on the behavior of the two-body energies, the fifth and sixth columns of Table II show the expectation value of H_{cm}, i.e., E_{NL} with $(NL) = (00)$, and the ground state expectation value of H_{rel} for the square well potential with $R_0 = 0.01a_{ho,1}$. The sum of these two expectation values coincides with the energy obtained for a single basis function [namely, $\Phi_{NLM_L}\phi_{nlm_l}$ with $(NLM_Lnlm_l) = (000000)$] in the diagonalization

TABLE II: Selected expectation values, in units of $\hbar\omega$, for the two-body system in the ground state with $N_1 = N_2 = 1$ at unitarity for $\kappa = 1$, 4 and 8 for various frequency ratios ω_2/ω_1. The energies in column 3 [superscript (1)] are calculated for the square well potential with $R_0 = 0.01 a_{ho,1}$ using the DMC method; in this case, the statistical uncertainty is in the last digit reported (or smaller). The expectation values in columns 4-6 [superscript (2)] are calculated for the square well potential with $R_0 = 0.01 a_{ho,1}$ using the diagonalization scheme. The energies in column 7 [superscript (3)] are obtained by extrapolating the energies obtained by the diagonalization scheme for various R_0 to the $R_0 \to 0$ limit; the extrapolation error is estimated to be at most $0.001\hbar\omega$.

κ	ω_2/ω_1	${E_{1,1}}^{(1)}$	${E_{1,1}}^{(2)}$	$\langle H_{cm}\rangle^{(2)}$	$\langle H_{rel}\rangle^{(2)}$	${E_{1,1}}^{(3)}$
1	1	2.003	2.002	1.500	0.502	2.000
	10/11	2.003	2.004	1.502	0.503	2.002
	10/13	2.014	2.014	1.513	0.506	2.012
	2/3	2.030	2.029	1.530	0.512	2.028
4	1	2.002	2.003	1.500	0.503	2.000
	3/4	1.927	1.927	1.382	0.549	1.924
	1/2	1.863	1.862	1.265	0.618	1.859
	1/4	1.867	1.866	1.200	0.725	1.863
	3/20	1.918	1.921	1.218	0.784	1.918
8	1	2.003	2.003	1.500	0.503	2.000
	3/4	1.898	1.898	1.340	0.560	1.895
	1/2	1.782	1.783	1.155	0.642	1.780
	1/4	1.700	1.701	0.980	0.761	1.697
	1/8	1.726	1.724	0.943	0.843	1.720

approach. The difference between the fully converged energies (column 4 of Table II) and this sum is due to the coupling between the center-of-mass and relative degrees of freedom. The expectation value of V_{coup} vanishes or is negative for all two-body systems considered in this work and its magnitude increases for a fixed κ with increasing $\omega_1 - \omega_2$. For $\kappa = 1$, the increase of $\langle H_{cm} + H_{rel}\rangle/(\hbar\omega)$ with increasing $\omega_1 - \omega_2$ is larger than the decrease of $\langle V_{coup}\rangle/(\hbar\omega)$; consequently, the equal-frequency system has the lowest energy. For $\kappa = 4$ and 8, $\langle H_{cm}\rangle/(\hbar\omega)$ first decreases with increasing $\omega_1 - \omega_2$ and then increases for $\omega_2/\omega_1 < 1/\kappa$, while the quantity $\langle H_{rel}\rangle/(\hbar\omega)$ increases with increasing $\omega_1 - \omega_2$ for all ω_2/ω_1. It can be determined readily that the energy of the two-body system at unitarity in the zero-range limit without the coupling, $(\omega_{rel}/2 + 3\omega_{cm}/2)/\omega$, is minimal at $\eta \approx 0.43$ and 0.54 for $\kappa = 4$ and 8, respectively. Since the absolute value of $\langle V_{coup}\rangle$ is fairly small compared to that of $\langle H_{cm} + H_{rel}\rangle$, the minimum of the energy $E_{1,1}/(\hbar\omega)$ shifts only slightly when the coupling term V_{coup} is included [see Fig. 2(a)].

The two-body system with unequal frequencies has been discussed previously by a number of groups. The energies of the lowest-lying gas-like states and the most weakly-bound molecular states of the trapped ^{40}K-^{87}Rb dimer have, e.g., been measured experimentally and been determined theoretically as part of a project on Fermi-Bose mixtures in a lattice [53]. Also, the effect of the coupling between the center-of-mass and relative motions has been investigated in the context of confinement-induced resonances [58, 59, 60]. Our main focus lies in extending the two-body study presented above to larger unequal-frequency systems with three, four or more particles per lattice site. While an increasing body of literature exists for larger equal-frequency systems, the regime where the center-of-mass motion does not decouple has, to the best of our knowledge, received only little attention for larger systems, despite its immediate relevance to ongoing experiments.

Figures 2(b) and (c) show the FN-DMC energies, in units of $\hbar\omega$, for two-component Fermi gases with $N = 3$ and 4 as a function of η for various mass ratios κ. The overall behavior of the $N = 4$ energies is similar to that of the $N = 2$ energies. For a given η, the $N = 4$ energies decrease with increasing κ. For $\kappa = 1$, the energy $E_{2,2}$ is minimal for $\eta \approx 0$ and increases with increasing $|\eta|$. As κ increases, $E_{2,2}$ is minimal for positive η values. As discussed above, the $N = 2$ eigenenergies for equal frequencies at unitarity approach $2\hbar\omega$ in the zero-range limit for all κ. For $N = 4$, in contrast, the energies at unitarity depend on the mass ratio even when the trapping frequencies coincide [46].

The $N = 3$ energies at unitarity behave qualitatively different from the $N = 2$ and 4 energies. For systems with one spare heavy atom [symbols connected by dotted lines in Fig. 2(b)], the energy for a given κ decreases with decreasing η. For systems with one spare light atom, the behavior is reversed, i.e., the energy increases with decreasing η. This behavior is similar to that of the coefficients $C_{1,2}$ and $C_{2,1}$ (see Fig. 1), and can qualitatively, as in the perturbative regime, be explained in terms of the overlap of the densities of the two components.

Table III summarizes selected FN-DMC energies for $N = 3 - 6$ at unitarity calculated for the square well potential with $R_0 = 0.01 a_{ho,1}$. The $N = 4$ energies for $\eta = 0$ and $\kappa = 4$ and 8 are slightly lower than those reported in Ref. [45]. This is due to the fact that the $\kappa > 1$ calculations of Ref. [45] for even N were restricted to the guiding function ψ_{T1}, while this paper also considers the guiding function ψ_{T2}, whose nodal surface coincides with that of the non-interacting system. For $N = 4$ and $\eta = 0$, the energies obtained using ψ_{T2} are lower than those obtained using ψ_{T1}. Table III also indicates the total angular momentum L_{tot} of the lowest energy state obtained by the FN-DMC method. For $N = 4$ and 6 (no superscript in Table III), we obtain the lowest energy for a guiding function with $L_{tot} = 0$ for all mass and trapping frequency ratios considered. For $N = 3$, in contrast, the total angular momentum of the lowest energy state depends on the system considered and is either 0 or 1. For $N = 5$, the lowest energy state found by the FN-DMC method has $L_{tot} = 1$.

To investigate the "angular momentum crossover" of the three-particle system with two light atoms and one heavy atom in more detail, Fig. 3 shows the FN-DMC

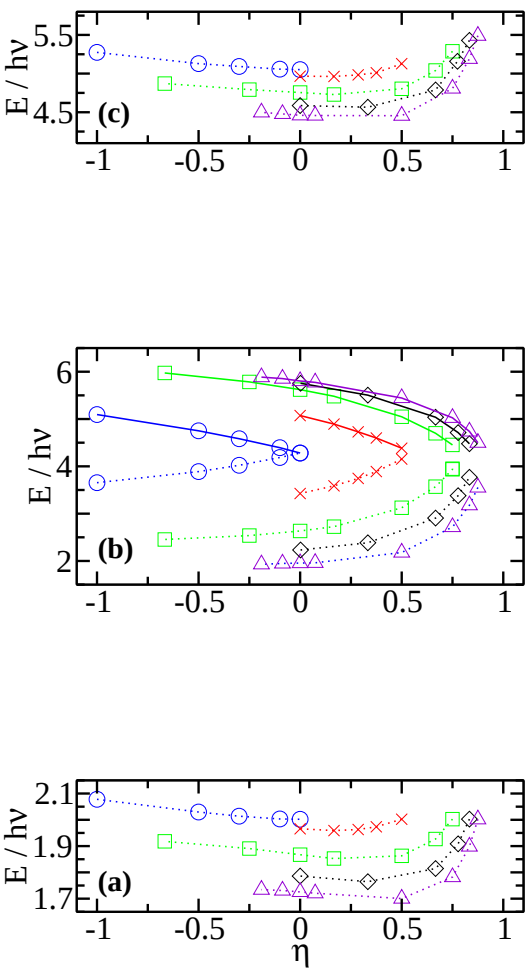

FIG. 2: (Color online) Ground state energies in units of $\hbar\omega$ for two-component Fermi gases at unitarity as a function of η for (a) $N = 2$, (b) $N = 3$ and (c) $N = 4$ for various mass ratios κ for the square well potential with $R_0 = 0.01a_{ho,1}$. The energies for $N = 2$ are calculated by the DMC method and those for $N = 3$ and 4 by the FN-DMC method. The energies for $\kappa = 1$, 2, 4, 6 and 8 are shown by circles, crosses, squares, diamonds and triangles, respectively. For a given κ, symbols are connected by lines to guide the eye: Dotted lines are used for $N = 2$, $N = 3$ with two heavy atoms and one light atom, and $N = 4$. Solid lines are used for $N = 3$ with two light atoms and one heavy atom. For $\kappa = 1$ and $N = 3$, the dotted (solid) line connects the energies for systems in which two particles feel the smaller (larger) trapping frequency. For each κ, the energies for the largest η value considered correspond to $\omega_1 = \omega_2$.

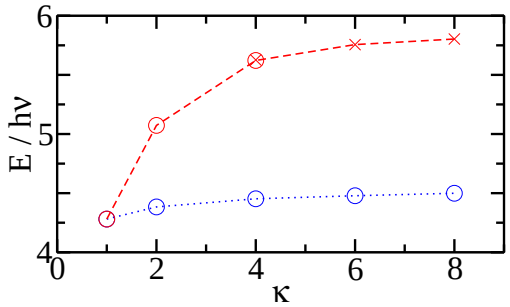

FIG. 3: (Color online) Ground state energies for $N = 3$ (two light atoms and one heavy atom) in units of $\hbar\omega$ as a function of κ at unitarity; the energies are calculated by the FN-DMC method for the square well potential with $R_0 = 0.01a_{ho,1}$. The symbols connected by dotted and dashed lines are calculated for equal trapping frequencies and equal trapping lengths, respectively. The energies shown by circles and crosses correspond to states with total angular momentum $L_{tot} = 1$ and 0, respectively.

energies for equal frequencies (symbols connected by a dotted line) and for equal trapping lengths (symbols connected by a dashed line) as a function of the mass ratio κ. Energies of states with $L_{tot} = 1$ and 0 are shown by circles and crosses, respectively. For equal trapping frequencies, the angular momentum of the lowest energy state is $L_{tot} = 1$ for all mass ratios considered. For equal trapping lengths, in contrast, L_{tot} changes from 1 to 0 at $\kappa \approx 4$. This angular momentum crossover has also been observed in calculations that employ the correlated Gaussian (CG) approach [61].

Figure 4 shows the energies for $N = 2 - 6$ with $\kappa = 4$ and 8 as a function of η. The energies for $N = 2$, 4 and 6 behave similarly as a function of η, with the $N = 2$ energies being nearly constant [see also Fig. 2(a)] and the $N = 4$ and 6 energies showing a stronger decrease than the $N = 2$ energies as η decreases from 3/4 to ≈ 0.4 for $\kappa = 4$ and from 7/8 to ≈ 0.5 for $\kappa = 8$ [see also the discussion in the context of Figs. 2(b) and (c)]. Furthermore, the energies $E_{2,1}$ and $E_{3,2}$, and the energies $E_{1,2}$ and $E_{2,3}$ show a similar overall behavior. The ordering of the energy levels for equal trapping frequencies (for $\kappa = 4$, e.g., this corresponds to $\eta = 3/4$) is, from bottom to top, $E_{1,1}$, $E_{1,2}$, $E_{2,1}$, $E_{2,2}$, $E_{2,3}$, $E_{3,2}$ and $E_{3,3}$. This ordering changes as η decreases; for $\kappa = 4$, e.g., $E_{2,1}$ becomes larger than $E_{2,2}$ at $\eta \approx 0.6$, and also larger than $E_{2,3}$ at $\eta \approx -0.2$. Similarly, $E_{3,2}$ becomes larger than $E_{3,3}$ at $\eta \approx 0.4$.

The small N energies can be combined to predict the energetically most favorable configuration of an optical

TABLE III: Selected FN-DMC energies E_{N_1,N_2}, in units of $\hbar\omega$, for $N = 3-6$ ($|N_1 - N_2| \leq 1$) at unitarity for $\kappa = 4$ and 8. The FN-DMC energies are uncertain in the last digit reported. The guiding functions used to obtain the energies marked by a superscript "$*$" have total angular momentum $L_{tot} = 1$ and those not marked by a superscript have $L_{tot} = 0$. The superscript "?" marks systems for which guiding functions with $L_{tot} = 0$ and 1 result in energies that are indistinguishable within the statistical uncertainties. For comparison, the CG approach results in $E_{2,1} = 5.67\hbar\omega$, $E_{1,2} = 1.96\hbar\omega$ and $E_{2,2} = 4.45\hbar\omega$ for $\kappa = 8$, $\omega_2/\omega_1 = 1/8$ and a range comparable to that employed in the FN-DMC calculations [61]; as in the equal-frequency case [42, 45, 46], the FN-DMC energies compare favorably with the energies calculated by the CG approach.

κ	ω_2/ω_1	$E_{2,1}$	$E_{1,2}$	$E_{2,2}$	$E_{3,2}$	$E_{2,3}$	$E_{3,3}$
4	1	4.45^*	3.94^*	5.29	7.99^*	7.44^*	9.51
	3/4	4.70^*	3.57^*	5.04	8.08^*	6.88^*	8.94
	1/2	5.05^*	3.13^*	4.80	8.26^*	6.27^*	8.44
	1/4	$5.62^?$	2.63^*	4.76	8.81^*	5.72^*	8.24
	3/20	$5.97^?$	2.45^*	4.87	9.24^*	5.62^*	8.43
8	1	4.50^*	3.55^*	5.49	8.19^*	7.12^*	9.59
	3/4	4.74	3.18^*	5.19	8.25^*	6.64^*	9.21
	1/2	5.03	2.72^*	4.81	8.31^*	5.90^*	8.78
	1/4	5.44	2.18^*	4.46	8.56^*	5.08^*	7.90
	1/8	5.80	1.96^*	4.46	8.96^*	4.83^*	7.82

lattice with small tunneling amplitude, approximately harmonic lattice sites, twice as many particles of one species than of the other and a filling factor equal to or smaller than 3/2. For equal masses and equal trapping frequencies, it has been shown previously for all a_s [41, 46, 62] that it is energetically more favorable for one spin-up and one spin-down atom to occupy one lattice site and for the second spin-down atom to occupy a different site [we refer to this as the "(2+1)-configuration"] than for the one spin-up and the two spin-down fermions to occupy the same lattice site [we refer to this as the "(3+0)-configuration"]. Figure 5 extends this analysis to trap- and mass-imbalanced systems at unitarity. A dotted line shows the energy of the (2+1)-configuration for $\kappa = 1$ at unitarity as a function of η [the particle in the singly-occupied lattice site feels the larger (smaller) frequency for $\eta > 0$ ($\eta < 0$)], while squares show the energy of the (3+0)-configuration. No crossing between these two curves is observed, with the energy of the (3+0)-configuration being larger than the energy of the (2+1)-configuration. We find a similar behavior for $\kappa = 4$: For the frequency ratios considered, the energy increase due to placing two like fermions in the same lattice site is so large that it is more favorable to place the like fermion in a separate lattice site instead (and thereby "loosing" the energy decrease due to having two like fermions interact with the unlike fermion through an attractive two-body potential). For $\kappa = 8$, however, the behavior is different: Figure 5 shows that

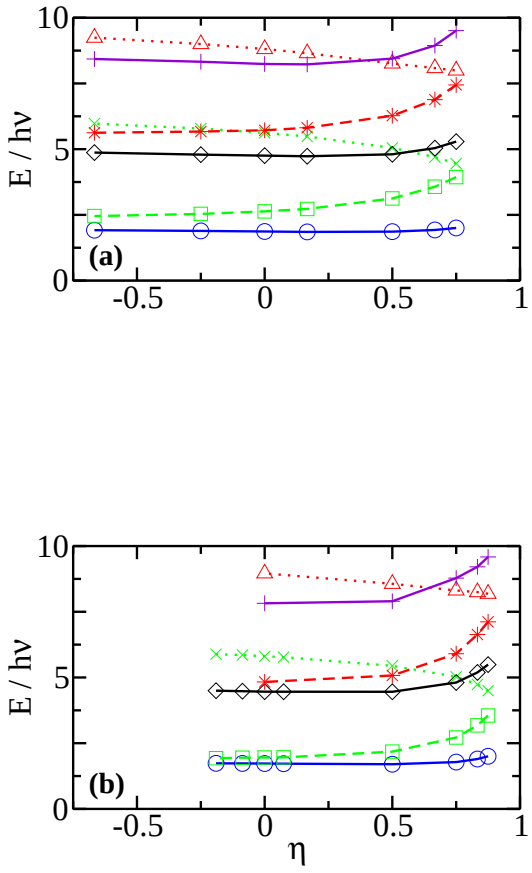

FIG. 4: (Color online) Ground state energies at unitarity for (a) $\kappa = 4$ and (b) $\kappa = 8$ as a funcion of η for $N = 2$ (circles), $N = 3$ (squares and crosses), $N = 4$ (diamonds), $N = 5$ (asterisks and triangles) and $N = 6$ (pluses). Energies for even N systems are connected by solid lines, and those for odd N systems with a spare heavy and a spare light particle by dashed and dotted lines, respectively. The calculations are performed using the DMC ($N = 2$) and the FN-DMC ($N = 3-6$) method for the square well potential with $R_0 = 0.01a_{ho,1}$.

the (2+1)-configuration (solid line) is energetically favorable for larger η and the (3+0)-configuration (circles) is energetically favorable for smaller η. The crossover is predicted to occur at $\eta \approx 0.8$. This suggests that it might be possible to introduce a macroscopic phase transition of an optical lattice system by changing the trapping frequency felt by one of the species if the mass ratio is sufficiently large but not necessarily so large that three-body bound states with molecular character exist.

We now discuss the odd-even oscillations of larger trapped unequal-mass systems at unitarity. In particular, we focus on systems with $\eta = 0$, i.e., on systems for

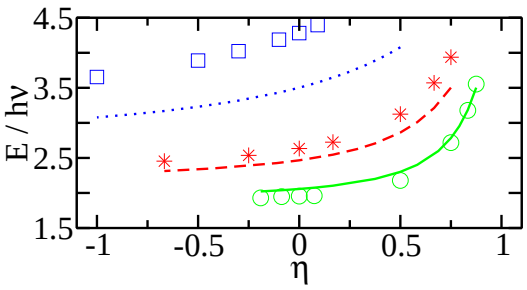

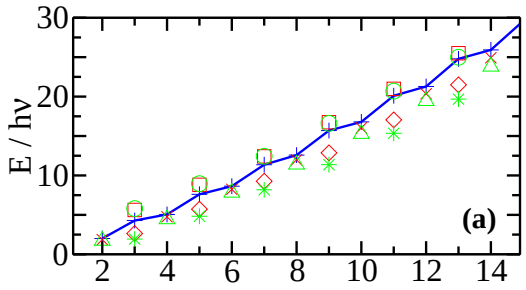

FIG. 5: (Color online) Comparison of the energies at unitarity for the (3+0)-configuration calculated by the FN-DMC method (symbols) and those for the (2+1)-configuration calculated by the diagonalization scheme (lines) as a function of η. The energies for the (3+0)-configuration are shown by squares, asterisks and circles for $\kappa = 1$, 4 and 8, respectively, while those for the (2+1)-configuration are shown by a dotted, dashed and solid line for $\kappa = 1$, 4 and 8, respectively. For $\kappa = 1$, two particles feel the larger (smaller) angular trapping frequency for $\eta > 0$ ($\eta < 0$); for $\kappa > 1$, the systems considered consist of two heavy fermions and one light fermion.

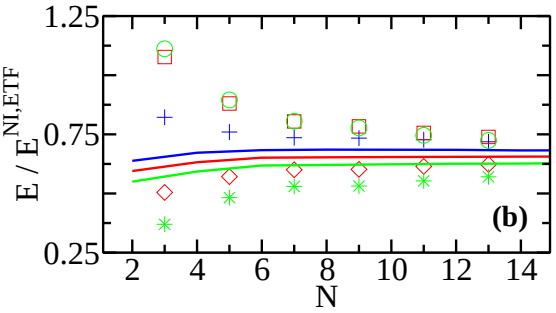

FIG. 6: (Color online) Energies in units of (a) $\hbar\omega$ and (b) $E^{NI,ETF}$ at unitarity for $\eta = 0$ as a function of N for $\kappa = 1$, 4 and 8. The energies are calculated for the square well potential with $R_0 = 0.01 a_{ho,1}$ using the DMC ($N = 2$) and FN-DMC ($N = 3-14$) methods. (a) $\kappa = 1$ (pluses connected by a solid line), $\kappa = 4$ [crosses for even N, and diamonds (spare heavy atom) and squares (spare light atom) for odd N], and $\kappa = 8$ [triangles for even N, and asterisks (spare heavy atom) and circles (spare light atom) for odd N]. (b) $\kappa = 1$ (uppermost solid line for even N and pluses for odd N), $\kappa = 4$ [middle solid line for even N, and diamonds (spare heavy atom) and squares (spare light atom) for odd N], and $\kappa = 8$ [lowermost solid line for even N, and asterisks (spare heavy atom) and circles (spare light atom) for odd N].

which the two oscillator lengths $a_{ho,1}$ and $a_{ho,2}$ coincide. Equal-mass systems with both even and odd N have already been discussed in Refs. [44, 46] and unequal-mass systems with even N in Ref. [45]. Results for unequal-mass systems with odd N ($N \geq 5$), in contrast, have not been presented before. For even N, $N \geq 6$, we obtain the lowest FN-DMC energy for $\kappa = 1$, 4 and 8 for the guiding function ψ_{T1} (see Sec. II B), whose nodal surface is constructed by anti-symmetrizing a two-body pair function. For odd N, we find that the guiding function that results in the lowest FN-DMC energy depends not only on N but also on κ: For $\kappa = 1$, the guiding function ψ_{T2} results in the lowest FN-DMC energy for $N \leq 9$, ψ_{T3} for $N = 11$ and ψ_{T1} for $N \geq 13$. For $\kappa = 4$ and 8 systems with a spare light atom, the guiding functions ψ_{T2} and ψ_{T1} result in the lowest FN-DMC energy for $N \leq 7$ and $N \geq 9$, respectively. For $\kappa = 4$ and 8 systems with a spare heavy atom, in contrast, the guiding functions ψ_{T2} and ψ_{T3} result in the lowest FN-DMC energy for $N \leq 9$ and $N \geq 11$, respectively. The density profiles reveal that the spare particle of the odd-N systems with $N \gtrsim 11$ and $\kappa = 1$ is located predominantly near the edge of the cloud [44, 46]. Thus, one may consider the core region as "fully paired" and the edge region as "partially paired". For $\kappa > 1$ systems with a spare heavy fermion, the pairing function ψ_{T1} results in a higher energy than ψ_{T3} for $N \geq 9$, suggesting that the nodal surface ψ_{T3} allows for a higher probability of three fermions to be in close proximity than the nodal surface of ψ_{T1} (recall, for sufficiently large κ three-body bound states with one quantum of angular momentum exist).

Figures 6(a) and (b) show the energies for systems with up to $N = 14$ atoms with $\kappa = 1$, 4 and 8. The even-N energies, shown in units of $\hbar\omega$ in Fig. 6(a), decrease for a given N with increasing κ [for $N = 2$ and 4, see also Figs. 2(a) and (c)]. The energies for systems with a spare

heavy particle (diamonds and asterisks for $\kappa = 4$ and 8, respectively) are notably smaller than the corresponding odd N energies for $\kappa = 1$. The energies for systems with a spare light particle (squares and circles for $\kappa = 4$ and 8, respectively), in contrast, are higher than the corresponding energies for $\kappa = 1$ for small N and nearly coincide with the corresponding energies for $\kappa = 1$ for larger N. Further optimization of the nodal surface of the guiding functions employed in the FN-DMC calculations may result in tighter upper bounds for the energies; a more detailed investigation of larger odd-N systems with $\kappa > 1$ is relegated to the future.

To see the odd-even oscillations more clearly, Fig. 6(b) scales the energies from panel (a) by the "smoothed" extended Thomas-Fermi energies $E^{NI,ETF}$ of the non-interacting system [63],

$$E^{NI,ETF} = \hbar\omega \frac{(3N)^{4/3}}{4}\left[1 + \frac{(3N)^{-2/3}}{2}\right]. \qquad (22)$$

For $\kappa = 1$, the scaled energies follow two distinct curves; the curve for odd N (pluses) is higher than that for even N (topmost solid line), reflecting the non-vanishing excitation gap at unitarity (see below and Refs. [43, 44, 46]). For fixed N, the scaled even-N energies decrease with increasing κ [45]. The scaled energies for odd-N systems with one spare heavy atom are lower than the corresponding scaled energies for systems with $N-1$ fermions and the same κ. The scaled energies for odd-N systems with one spare light particle, in contrast, are higher than the corresponding scaled energies for systems with $N-1$ fermions and the same κ.

Next, we combine our energies for even and odd N to determine the excitation gap $\Delta(N)$, Eq. (19), at unitarity. Figure 7 shows $\Delta(N)$ for $N = 3$ as a function of η for various κ. Although the FN-DMC energies themselves provide an upper bound to the exact eigenenergies, the excitation gap is not variational. Figure 7 shows that the excitation gap $\Delta(3)$ for $\kappa = 1$ through 8 collapse—for the systems considered—approximately to a single curve for $\eta \gtrsim 0$; $\Delta(3)$ is maximal around $\eta = 0$ and decreases with increasing η. While more detailed calculations may reveal the dependence of $\Delta(3)$ on κ for a given η in more detail, our calculations suggest that $\Delta(3)$ is determined predominantly by η and only secondarily by κ. This is in contrast to the energies themselves (see, e.g., Fig. 2) and can be attributed at least partially to the fact that the energies of the two odd-N systems (that with a spare heavy and that with a spare light particle) enter into $\Delta(3)$ as an averaged quantity.

For larger N, we determine the excitation gap $\Delta(N)$ at unitarity for $\kappa = 1$, 4 and 8 for systems with equal trapping lengths, i.e., for $a_{ho,1} = a_{ho,2}$. Figure 8 shows that $\Delta(N)$, expressed in units of $\hbar\omega$, is nearly constant ($\approx 0.75\hbar\omega$) for $N = 3, 5$ and 7 for all mass ratios considered (for $N = 3$, see also Fig. 7). For $N \geq 9$, the excitation gap $\Delta(N)$ is largest for $\kappa = 1$ and smallest for $\kappa = 8$. Despite the fairly large uncertainties of the excitation gap (see caption of Fig. 8), we are quite confident that the excitation gap does indeed decrease with increasing κ but fixed N ($N \gtrsim 9$). This is a direct consequence of the decrease of the energies for odd-N systems with a spare heavy particle with increasing κ.

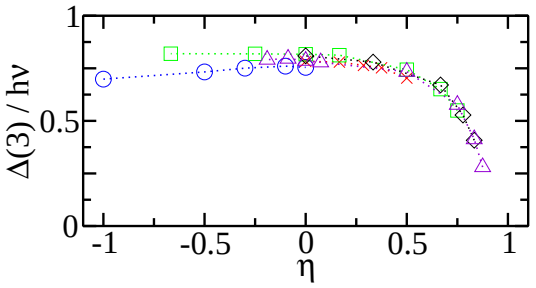

FIG. 7: (Color online) Excitation gap $\Delta(3)$ in units of $\hbar\omega$ as a function of η for two-component Fermi gases at unitarity for various κ. The $\Delta(3)$, calculated using the DMC ($N = 2$) and FN-DMC ($N = 3$ and 4) energies, are shown by circles, crosses, squares, diamonds and triangles for $\kappa = 1$, 2, 4, 6 and 8, respectively. Dotted lines connect symbols for a fixed κ to guide the eye.

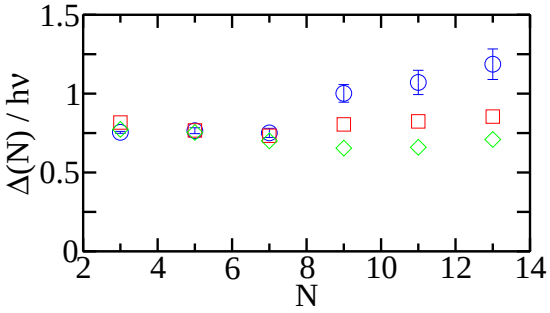

FIG. 8: (Color online) Excitation gap $\Delta(N)$ in units of $\hbar\omega$ at unitarity for $\eta = 0$ (i.e., for $m_1\omega_1 = m_2\omega_2$) as a function of N for $\kappa = 1$ (circles with errorbars), $\kappa = 4$ (squares), and $\kappa = 8$ (diamonds). The errorbars of $\Delta(N)$ for $\kappa = 4$ and 8, which are not shown to enhance the clarity of the figure, are a bit larger than those for $\kappa = 1$. The excitation gap $\Delta(N)$ is calculated from the energies shown in Fig. 6.

C. Small positive s-wave scattering length

This section discusses the behavior of two-component Fermi gases with unequal masses and unequal frequencies in the BEC regime where the s-wave scattering length a_s is small and positive. In this regime, the behavior of the molecular Bose gas is expected to be governed by the dimer-dimer scattering length a_{dd} [19, 64, 65]. For equal-frequency systems, the four-fermion spectrum has been compared with that of two bosons [45, 46], validating the "dimer picture". This section extends the previous analysis to two-component Fermi gases with unequal frequencies.

We determine the two-body energy $E_{1,1}$ for unequal frequency systems using the diagonalization scheme. For a sufficiently small atom-atom scattering length, we find that the two-body energy is to a very good approximation given by the sum of the expectation values of H_{cm} and H_{rel} (the expectation value of the coupling term V_{coup} is smaller than $10^{-4}\hbar\omega$ for the systems considered in Fig. 9). Thus, an approximate but highly accurate expression for the ground state energy of the two-body system on the BEC side reads

$$E_{1,1} \approx \langle H_{rel}\rangle_{000} + \frac{3}{2}\hbar\omega_{cm}. \tag{23}$$

Assuming diatomic molecules form, the lowest energy of the four-particle system with $N_1 = N_2 = 2$ and small a_s can be written as

$$E_{2,2} \approx 2\langle H_{rel}\rangle_{000} + \frac{3}{2}\hbar\omega_{cm} + E_{rel,boson}, \tag{24}$$

where the first term on the right hand side is the internal energy of the two bosonic molecules, the second term on the right hand side is the center-of-mass energy of the two-boson system and the third term on the right hand side is the relative energy of the two-boson system. We rewrite the latter as

$$E_{rel,boson} = \frac{3}{2}\hbar\omega_{cm} + E_{dd}, \tag{25}$$

and evaluate the "dimer-dimer interaction shift" E_{dd} in first order perturbation theory (assuming a Fermi contact potential) [50, 57],

$$E_{dd} \approx \sqrt{\frac{2}{\pi}}\,\frac{a_{dd}}{a_{ho,cm}}\,\hbar\omega_{cm}. \tag{26}$$

Here, $a_{ho,cm}$ denotes the oscillator length associated with ω_{cm}, i.e., $a_{ho,cm} = \sqrt{\hbar/(M\omega_{cm})}$. It follows that the energy difference $E_{2,2} - 2E_{1,1}$ should be given by the interaction shift E_{dd}. The reasoning outlined here for four fermions can be extended to larger systems: The trapping frequency ω_{rel} determines—together with the atom-atom scattering length a_s—the internal binding energy of the molecules while the trapping frequency ω_{cm} determines—together with the dimer-dimer scattering length a_{dd}—the properties of the composite boson system.

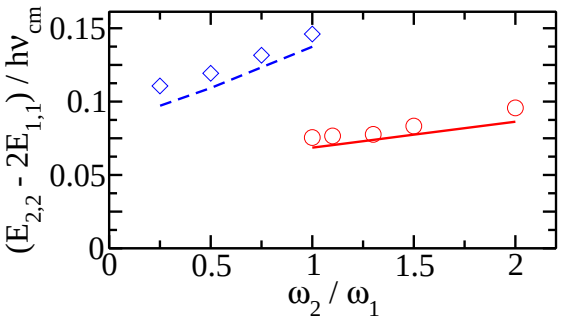

FIG. 9: (Color online) Interaction shifts in units of $\hbar\omega_{cm}$ for four-particle system in the BEC regime. Circles and diamonds show the energy difference $E_{2,2} - 2E_{1,1}$ for $\kappa = 1$ and 4, respectively; the uncertainty of $(E_{2,2} - 2E_{1,1})/(\hbar\omega_{cm})$ is about $0.01\hbar\omega_{cm}$. The energies $E_{2,2}$ and $E_{1,1}$ are calculated by the FN-DMC and diagonalization approaches, respectively, for the square well potential with $R_0 = 0.01a_{ho,1}$ and $a_s = 0.1a_{ho,1}$. For comparison, solid and dashed lines show the interaction shift E_{dd} determined perturbatively, Eq. (26), for $\kappa = 1$ and 4, respectively. The quantity $a_s/a_{ho,cm}$ increases with increasing ω_2/ω_1, which explains the increase of the interaction shift with increasing ω_2/ω_1.

Figure 9 shows the difference between the FN-DMC energy $E_{2,2}$ and twice the two-body energy $E_{1,1}$ as a function of the frequency ratio ω_2/ω_1 for $\kappa = 1$ (circles) and $\kappa = 4$ (diamonds). For comparison, solid and dashed lines show the interaction shift E_{dd}, Eq. (26), for $\kappa = 1$ (using $a_{dd} = 0.608a_s$ [45, 46, 64, 66]) and $\kappa = 4$ (using $a_{dd} = 0.77a_s$ [19, 45, 46]), respectively. The numerically determined energy differences are a bit larger than the perturbative result, which is in agreement with the fact that the FN-DMC energy $E_{2,2}$ provides an upper bound to the true eigenenergy [52]. The agreement between the interaction shift obtained by solving the full four-body Schrödinger equation and by treating the weakly-interacting two-boson system perturbatively is similarly good for all trapping frequencies considered. This confirms that the relevant "boson frequency" is indeed, as has been argued previously by others [24, 47], given by ω_{cm}.

IV. CONCLUSION

This paper determines the ground state energies of two-component Fermi systems under external harmonic confinement with unequal masses and unequal frequencies. We considered the weakly-interacting, small $|a_s|$ regime with both positive and negative scattering lengths

a_s as well as the strongly-interacting unitary regime where the s-wave scattering length diverges. In all three regimes, we identified convenient energy and length units. In the weakly-attractive regime, we treated the atomic Fermi gas perturbatively. In the unitary regime, we determined the eigenenergies numerically. In the weakly-repulsive regime, we compared numerical results with those obtained by treating the weakly-repulsive molecular Bose gas perturbatively.

The calculations at unitarity are performed for a short-range potential with small range; the resulting energies are estimated to be quite close to the zero-range limit. We determine the energies as a function of both the ratio between the masses of the two species and the ratio between the trapping frequencies felt by the two species. The small N results presented cover a wide range of mass and frequency ratios and can easily be extrapolated to experimentally relevant parameter combinations (such as ^{6}Li-^{40}K mixtures). Our FN-DMC energies provide an upper bound to the true ground state energy of mass- and trap-imbalanced two-component Fermi systems and may be serve as a benchmark for other approaches.

DB is grateful to J. von Stecher for calculating the CG energies reported in the caption of Table III and for discussions during the initial stage of this work. DB also gratefully acknowledges support by the NSF through grant PHY-0555316.

[1] J. M. McNamara, T. Jeltes, A. S. Tychkov, W. Hogervorst, and W. Vassen, Phys. Rev. Lett. **97**, 080404 (2006).
[2] A. G. Truscott, K. E. Strecker, W. I. McAlexander, G. B. Partridge, and R. G. Hulet, Science **291**, 2570 (2001).
[3] B. DeMarco and D. S. Jin, Science **285**, 1703 (1999).
[4] T. Fukuhara, Y. Takasu, M. Kumakura, and Y. Takahashi, Phys. Rev. Lett. **98**, 030401 (2007).
[5] T. Fukuhara, Y. Takasu, S. Sugawa, and Y. Takahashi, J. Low Temp. **148**, 441 (2007).
[6] G. Modugno, G. Roati, F. Riboli, F. Ferlaino, R. J. Brecha, and M. Inguscio, Science **297**, 2240 (2002).
[7] J. Goldwin, S. Inouye, M. L. Olsen, B. Newman, B. D. DePaola, and D. S. Jin, Phys. Rev. A **70**, 021601 (2004).
[8] M. Modugno, F. Ferlaino, F. Riboli, G. Roati, G. Modugno, and M. Inguscio, Phys. Rev. A **68**, 043626 (2003).
[9] C. Ospelkaus, S. Ospelkaus, K. Sengstock, and K. Bongs, Phys. Rev. Lett. **96**, 020401 (2006).
[10] J. P. Gaebler, J. P. Stewart, J. L. Bohn, and D. S. Jin, Phys. Rev. Lett. **98**, 200403 (2007).
[11] M. Greiner, C. A. Regal, and D. S. Jin, Nature **426**, 537 (2003).
[12] M. W. Zwierlein, C. A. Stan, C. H. Schunck, S. M. F. Raupach, S. Gupta, Z. Hadzibabic, and W. Ketterle, Phys. Rev. Lett. **91**, 250401 (2003).
[13] K. E. Strecker, G. B. Partridge, and R. G. Hulet, Phys. Rev. Lett. **91**, 080406 (2003).
[14] M. Taglieber, A.-C. Vogt, F. Henkel, S. Fray, T. W. Hänsch, and K. Dieckmann, Phys. Rev. A **73**, 011402(R) (2006).
[15] M. Taglieber, A.-C. Vogt, T. Aoki, T. W. Hänsch, and K. Dieckmann, Phys. Rev. Lett. **100**, 010401 (2008).
[16] see, e.g., http://www.uibk.ac.at/exphys/ultracold/.
[17] V. Efimov, Yad. Fiz. **12**, 1080 (1970) [Sov. J. Nucl. Phys. **12**, 598 (1971)].
[18] V. N. Efimov, Nucl. Phys. A **210**, 157 (1973).
[19] D. S. Petrov, C. Salomon, and G. V. Shlyapnikov, J. Phys. B **38**, S645 (2005).
[20] O. I. Kartavtsev and A. V. Malykh, J. Phys. B **40**, 1429 (2007).
[21] S.-T. Wu, C.-H. Pao, and S.-K. Yip, Phys. Rev. B **74**, 224504 (2006).
[22] M. Iskin and C. A. R. Sá de Melo, Phys. Rev. Lett. **97**, 100404 (2006).
[23] G.-D. Lin, W. Yi, and L.-M. Duan, Phys. Rev. A **74**, 031604(R) (2006).
[24] G. Orso, L. P. Pitaevskii, and S. Stringari, Phys. Rev. A **77**, 033611 (2008).
[25] M. M. Parish, F. M. Marchetti, A. Lamacraft, and B. D. Simons, Phys. Rev. Lett. **98**, 160402 (2007).
[26] M. Iskin and C. A. R. Sá de Melo, Phys. Rev. A **77**, 013625 (2008).
[27] Y. Nishida, D. T. Son, and S. Tan, Phys. Rev. Lett. **100**, 090405 (2008).
[28] W. C. Stwalley, Phys. Rev. Lett. **37**, 1628 (1976).
[29] E. Tiesinga, B. J. Verhaar, and H. T. C. Stoof, Phys. Rev. A **47**, 4114 (1993).
[30] S. Inouye, M. R. Andrews, J. Stenger, H. J. Miesner, D. M. Stamper-Kurn, and W. Ketterle, Nature **392**, 151 (1998).
[31] S. L. Cornish, N. R. Claussen, J. L. Roberts, E. A. Cornell, and C. E. Wieman, Phys. Rev. Lett. **85**, 1795 (2000).
[32] M. Greiner, O. Mandel, T. Esslinger, T. W. Hänsch, and I. Bloch, Nature **415**, 39 (2002).
[33] T. Stöferle, H. Moritz, C. Schori, M. Köhl, and T. Esslinger, Phys. Rev. Lett. **92**, 130403 (2004).
[34] M. Köhl, H. Moritz, T. Stöferle, K. Günter, and T. Esslinger, Phys. Rev. Lett. **94**, 080404 (2005).
[35] T. Rom, T. Best, D. van Oosten, U. Schneider, S. Fölling, B. Paredes, and I. Bloch, Nature **444**, 733 (2006).
[36] R. P. Feynman, Int. J. Theor. Phys. **21**, 467 (1982).
[37] S. Lloyd, Science **273**, 1073 (1996).
[38] E. Jané, G. Vidal, W. Dür, P. Zoller, and J. I. Cirac, Quantum Information and Computation **3**, 15 (2003).
[39] F. Werner and Y. Castin, Phys. Rev. Lett. **97**, 150401 (2006).
[40] R. Jáuregui, R. Paredes, and G. Toledo Sánchez, Phys. Rev. A **76**, 011604(R) (2007).
[41] J. P. Kestner and L.-M. Duan, Phys. Rev. A **76**, 033611 (2007).
[42] J. von Stecher and C. H. Greene, Phys. Rev. Lett. **99**, 090402 (2007).
[43] S. Y. Chang and G. F. Bertsch, Phys. Rev. A **76**, 021603(R) (2007).
[44] D. Blume, J. von Stecher, and C. H. Greene, Phys. Rev. Lett. **99**, 233201 (2007).
[45] J. von Stecher, C. H. Greene, and D. Blume, Phys. Rev.

A **76**, 053613 (2007).
[46] J. von Stecher, C. H. Greene, and D. Blume, arXiv:0801.2747 (to appear in Phys. Rev. A).
[47] M. Iskin and C. J. Williams, Phys. Rev. A **77**, 013605 (2008).
[48] M. W. Zwierlein, C. H. Schunck, A. Schirotzek, and W. Ketterle, Nature **442**, 54 (2006).
[49] G. P. Partridge, W. H. Li, R. I. Kamar, Y. A. Liao, and R. G. Hulet, Science **311**, 503 (2006).
[50] E. Fermi, Nuovo Cimento **11**, 157 (1934).
[51] B. L. Hammond, W. A. Lester, Jr., and P. J. Reynolds, *Monte Carlo Methods in Ab Initio Quantum Chemistry* (World Scientific, Singapore, 1994).
[52] P. J. Reynolds, D. M. Ceperley, B. J. Alder, and W. A. Lester, Jr., J. Chem. Phys. **77**, 5593 (1982).
[53] F. Deuretzbacher, K. Plassmeier, D. Pfannkuche, F. Werner, C. Ospelkaus, S. Ospelkaus, K. Sengstock, and K. Bongs, cond-mat/0703322v3.
[54] K. Huang and C. N. Yang, Phys. Rev. **105**, 767 (1957).
[55] K. Kanjilal and D. Blume, Phys. Rev. A **73**, 060701(R) (2006).
[56] S. Giorgini, L. P. Pitaevskii, and S. Stringari, arXiv:cond-mat/0706.3360 (to appear in Rev. Mod. Phys.).
[57] T. Busch, B.-G. Englert, K. Rzążewski, and M. Wilkens, Foundations of Phys. **28**, 549 (1998).
[58] R. Stock, I. H. Deutsch, and E. L. Bolda, Phys. Rev. Lett. **91**, 183201 (2003).
[59] J. I. Kim and V. S. Melezhik and P. Schmelcher, Phys. Rev. Lett. **97**, 193203 (2006).
[60] V. S. Melezhik and J. I. Kim and P. Schmelcher, Phys. Rev. A **76**, 053611 (2007).
[61] J. von Stecher, private communication.
[62] I. Stetcu, B. R. Barrett, U. van Kolck, and J. P. Vary, Phys. Rev. A **76**, 063613 (2007).
[63] M. Brack and R. K. Bhaduri, *Semiclassical Physics* (Addison-Wesley, Reading, MA, 1997).
[64] D. S. Petrov, C. Salomon, and G. V. Shlyapnikov, Phys. Rev. Lett. **93**, 090404 (2004).
[65] D. S. Petrov, C. Salomon, and G. V. Shlyapnikov, Phys. Rev. A **71**, 012708 (2005).
[66] G. E. Astrakharchik, J. Boronat, J. D. Casulleras, and S. Giorgini, Phys. Rev. Lett. **93**, 200404 (2004).